The time-dependence of intense archeomagnetic flux patches

Hagay Amit,[1] Monika Korte,[2] Julien Aubert,[3] Catherine Constable,[4] and Gauthier Hulot[5]

Received 19 May 2011; revised 21 September 2011; accepted 6 October 2011; published 14 December 2011.

[1] The long-term temporal behavior of intense geomagnetic flux patches at the core-mantle boundary and the relation with lower mantle lateral heterogeneity are under debate. We apply an algorithm to detect centers of intense flux patches and track their time-evolution in a recent archeomagnetic field model in order to study the kinematics of such intense magnetic flux patches on millennial timescale. We find that most intense flux patches appear near the edge of the tangent cylinder. Quasi-stationary periods with small oscillations of patches occur more than drifts. Detailed comparison of the archeomagnetic patches' behavior with that seen in numerical dynamos with tomographic heat flux boundary conditions suggests that core-mantle thermal coupling could be the cause of a statistical preference for some longitudes on the long term, which does not exclude significant time spent away from the preferred longitudes. This could explain the roughly coincident locations of high-latitude patches in the historical geomagnetic field with that of the time-average paleomagnetic field together with the much weaker patches intensity in the latter. Alternating eastward and westward drifts are also observed. The drifts are more westward than eastward, especially in the southern hemisphere, indicating that the time-average zonal core flow may also be driven by core-mantle thermal coupling. An average patch lifetime of ~300 years is found, which we hypothesize may indicate the vortex lifetime in the outer core.

Citation: Amit, H., M. Korte, J. Aubert, C. Constable, and G. Hulot (2011), The time-dependence of intense archeomagnetic flux patches, *J. Geophys. Res.*, *116*, B12106, doi:10.1029/2011JB008538.

1. Introduction

[2] The geomagnetic field is generated by convective motion of an electrically conducting fluid in Earth's outer core. Measurements of the geomagnetic field and its secular variation (SV) provide vital constraints on the working of the geodynamo. The *gufm1* model [*Jackson et al.*, 2000] spanning the historical period shows that the geomagnetic field at the core-mantle boundary (CMB) is characterized by high-latitude intense flux patches. These patches also seem to appear in archeomagnetic field models over millennial timescale [*Korte and Constable*, 2005; *Korte et al.*, 2009] as well as in some paleomagnetic models representing the time-average field over the past five million years [*Kelly and Gubbins*, 1997]. Furthermore, intense high-latitude magnetic flux patches are reproduced by numerical dynamo simulations [*Christensen et al.*, 2010] where downwelling flow at the edge of the tangent cylinder concentrates field lines on the outer boundary [e.g., *Christensen et al.*, 1998].

[3] If the non-zonal structures in the paleomagnetic field models are indeed robust, the most natural way to explain preferential longitudes in the steady core field is by the impact of the heterogeneous mantle on the geodynamo. Numerical dynamo models with a heterogeneous heat flux outer boundary condition have indeed demonstrated that mantle control can affect the locations of intense magnetic flux patches on the CMB [*Bloxham*, 2002; *Olson and Christensen*, 2002; *Gubbins et al.*, 2007; *Aubert et al.*, 2008]. However, the time-dependence of these structures is under debate. In highly supercritical numerical dynamos with comparable thermal and magnetic diffusivities and no volumetric buoyancy sources or sinks, magnetic field structures are very mobile and the mantle signature appears clearly only in long-term time-averages over several magnetic diffusion times [*Bloxham*, 2002; *Olson and Christensen*, 2002]. In contrast, in slightly supercritical numerical dynamos with magnetic diffusivity an order of magnitude smaller than thermal diffusivity and a volumetric buoyancy source, magnetic field locking to the boundary heterogeneity is obtained and the patches are practically stationary [*Gubbins et al.*, 2007; *Willis et al.*, 2007].

[4] Recently, *Amit et al.* [2010], from hereafter AAH10, studied in detail the behavior of intense flux patches in highly supercritical numerical dynamos with heterogeneous CMB heat flux inferred from a lower mantle seismic tomography

[1]Laboratoire de Planétologie et de Géodynamique, Université de Nantes, CNRS UMR 6112, Nantes, France.
[2]Helmholtz-Zentrum Potsdam, Deutsches GeoForschungsZentrum, Potsdam, Germany.
[3]Equipe de Dynamique des Fluides Géologiques, Institut de Physique du Globe de Paris, Sorbonne Paris Cité, Université Paris Diderot, INSU, CNRS, UMR 7154, Paris, France.
[4]Institute for Geophysics and Planetary Physics, Scripps Institution of Oceanography, University of California, San Diego, La Jolla, California, USA.
[5]Equipe de Géomagnétisme, Institut de Physique du Globe de Paris, Sorbonne Paris Cité, Université Paris Diderot, INSU, CNRS, UMR 7154, Paris, France.

0148-0227/11/2011JB008538

model [*Masters et al.*, 2000]. They designed an algorithm to identify and track these magnetic structures. They found that the patches oscillate about preferred locations prescribed by the mantle heterogeneity with episodic drift events from one preferred location to another. The drift events were attributed to azimuthal motion of fluid downwelling structures that concentrate magnetic flux. They also observed more time-dependence in the southern hemisphere due to a stronger north-south shear in the mantle-driven zonal thermal wind there.

[5] In order to improve the understanding of the dynamics of intense flux patches in Earth's core and better constrain numerical dynamo models, a characterization of the behavior of intense geomagnetic flux patches over long time periods is necessary. Time-dependent archeomagnetic field models spanning millennial time-scales are the best available tool for that purpose. *Constable et al.* [2000] noticed that the patches in the past three millennia are mobile and not fully locked. This was confirmed in a recent study by *Korte and Holme* [2010], who investigated how much deviation from different time-average field configurations was required by a 7 kyr global data set. While the existence of both northern and southern hemisphere flux lobes proved compatible with the data in the time average field but not mandatory, they found evidence for considerable variability of these features on shorter timescales. *Dumberry and Finlay* [2007] focused on azimuthal motions of Earth's magnetic field features by investigating the time-dependent, non-zonal, high-pass filtered part of the field model *CALS7K.2* [*Korte and Constable*, 2005]. They visualized the azimuthal motions of these features by time-longitude plots and calculated the dominant azimuthal motions at each latitude using a technique based on the Radon transform [*Finlay and Jackson*, 2003]. They attributed most of the azimuthal motions to the mobility of the high-latitude intense flux patches in the northern hemisphere. *Wardinski and Korte* [2008] inverted the same field model and SV for the flow responsible for such changes at the top of the core. Their flow solutions represent 200-years time-averages (rather than snapshots) expanded up to degree 5, reflecting the limited temporal and spatial resolution of the archaeomagnetic field model. Such inversions might be severely biased by uncertainties in the archeomagnetic SV.

[6] This paper complements the previous ones by using a different approach and focusing on the dominant geomagnetic flux patches often found at high-latitudes. Here we apply the algorithm developed by AAH10 to the recent *CALS3k.3* archeomagnetic field model spanning the past three millennia to assess the behavior of the patches at the CMB. Thanks to a significantly increased data base, this model based on spherical harmonics in space and cubic B-splines in time exhibits higher resolution than its predecessors *CALS3k.1* [*Korte and Constable*, 2003] and *CALS3k.2* [*Korte and Constable*, 2005]. Particularly the southern hemisphere resolution has increased, although the amount of data from the northern hemisphere still dominates. The model is expanded to spherical harmonic degree 10 in space with a 10 year knot-point spacing of the splines, but the actual resolution is significantly lower. Archeo- and paleomagnetic data contain large uncertainties, both in the magnetic data themselves and in the age determination. Regularizations in both space and time have been applied in the modeling to trade off the fit to the data against what is assumed to be a realistic and robust amount of structure, based on the comparison of geomagnetic power spectra. We use the full field model to extract the kinematics of intense flux patches, including quasi-stationary periods. Our analysis enables tracking the 2D trajectory of the patches, i.e. both azimuthal and meridional motions. Analysis of the time series of patches coordinates allows quantifying the relative periods in which the patches are quasi-stationary or drifting, and their average and maximum lifetimes.

[7] The outline of the paper is as follows. In section 2 we recall the method of AAH10 for identifying and tracking intense patches on time series of snapshots. We refine their algorithm for compatibility with the larger scale archeomagnetic field models. In section 3 we present the results of our analysis. Comparison with previous studies, geophysical implications and consequences for data reliability assessment are discussed in section 4. We summarize our main findings in section 5.

2. Method

[8] Following the principles of the *connected component labeling* method previously used for detecting plumes in mantle convection simulations [*Labrosse*, 2002], AAH10 identified intense patches in images from numerical dynamos by searching grid points where the absolute radial magnetic field B_r on the outer boundary is larger than a critical threshold

$$|B_r(\phi,\theta)| > f_b |B_r(\phi,\theta)|_{\max} \tag{1}$$

where ϕ and θ are longitude and co-latitude spherical coordinates respectively. For the instantaneous small-scale dynamo field, AAH10 set $f_b = 0.6$. For the large-scale time-average fields, however, they used larger fractional values in order to adjust to the larger length-scales and different zonal components in the time-average maps. The identified extreme points were then grouped based on the spherical distance between one extreme point to another. Once all extreme points were assigned to a given group, a center of mass was calculated for each group. These centers of mass represent centers of intense flux patches.

[9] We use the recent *CALS3k.3* archeomagnetic field model of *Korte et al.* [2009] with a grid size of 5° in longitude and latitude. The snapshots in this lower resolution heavily damped field model resemble in terms of spatial scales the time-average dynamo fields. A low f_b value is therefore prone to produce large connectivity along high-latitude belts and therefore biased patch locations in some snapshots. A large f_b value, however, might leave some patches unidentified. We therefore use the non-zonal field B_r^{nz} to break the connectivity between the patches. Together with criterion (1), we also require

$$\left|B_r^{nz}(\phi,\theta)\right| > f_{nz} \left|B_r^{nz}(\phi,\theta)\right|_{\max} \tag{2}$$

restricting criterion (2) for normal polarity flux only.

[10] The identification method is demonstrated in Figure 1 with an arbitrary snapshot from *CALS3k.3* for $f_b = 0.7$ and $f_{nz} = 0.2$. The identified intense points (Figure 1a) are connected in the northern hemisphere through the polar region, so criterion (1) alone would cause erroneous patch

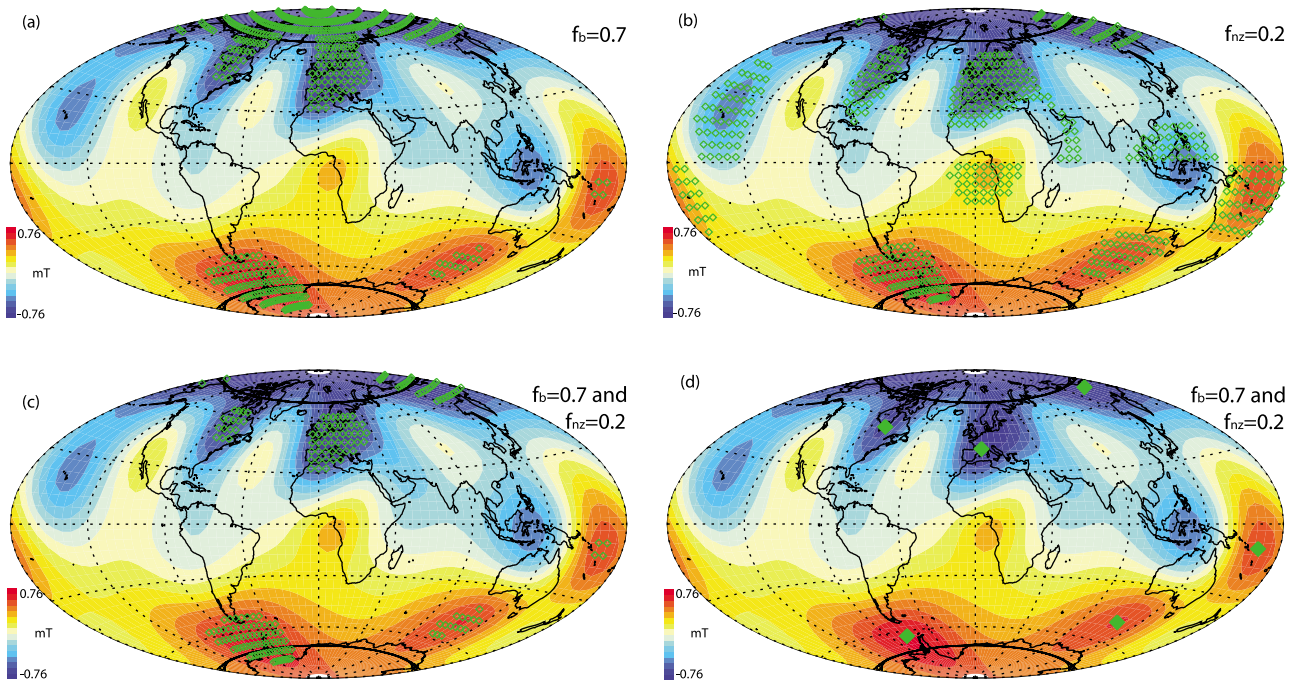

Figure 1. Demonstration of the patches identification method for the radial field B_r of the archeomagnetic model *CALS3k.3* in year −800. (a) Intense points based on criterion (1) with $f_b = 0.7$; (b) non-zonal points based on criterion (2) with $f_{nz} = 0.2$; (c) points that pass the two criteria; (d) the identified centers of patches. Identified points in Figures 1a–1c are denoted by small empty diamonds; Centers of identified patches in Figure 1d are denoted by large filled diamonds. Solid black lines mark the latitudes where the tangent cylinder intersects the CMB.

location there. The identified normal polarity non-zonal points (Figure 1b) readily separate the northern hemisphere lobes, but include many weak (mostly low-latitude) features in both hemispheres. The combination of the two criteria (Figure 1c) results in a satisfactory detection of the centers of mass of the intense flux patches (Figure 1d).

[11] Tracking of patches from one snapshot to the next is performed as in AAH10. Two patches in consecutive snapshots are labeled as the same patch if the spherical distance between them is smaller than a critical value that corresponds to an azimuthal distance $\delta^c = \omega^e \Delta t$, where $\omega^e \sim 0.2°$/yr is used as an upper bound longitudinal drift value based on inferred low-latitude fast drifting geomagnetic features [*Bloxham and Jackson*, 1991] and Δt is the time step.

[12] An analysis of the time series is performed following AAH10. First, we calculate the time-derivatives of the longitudes of the intense flux patches. Semi-stationary periods termed 'St' are characterized by small time-derivatives whereas drifts are characterized by large time-derivatives, with the threshold being $\delta^c/2\Delta t = \omega^e/2$. Integrated amounts of time of eastward and westward drifts are denoted by 'Ea' and 'We' respectively. The absolute RMS drift rates (without distinguishing east or west) are also reported. Second, we quantify the time-dependence of the patches by their average and maximum lifetimes τ_a and τ_m. Unlike AAH10, we avoid reporting probabilities of patches to be in a vicinity of a time-average patch because the time-average archeomagnetic field is expected to differ from the true long-term time-average field and calculating such probabilities would clearly be biased to large values. All quantities are given for each hemisphere separately. The results of the synthetic analysis are summarized in Table 1.

3. Results

[13] We first examine the locations of intense magnetic flux patches in time-average field models. In Figure 2a we applied our method for the time-average archeomagnetic

Table 1. Synthetic Analysis of *CALS3k.3* for Different f_b and Δt Values[a]

f_b	Δt	St	Ea	We	Ne	Rate	τ_a	τ_m	N_p
				NH					
0.7	50	83.1	2.4	14.5	−12.1	0.20	239	950	1.8
0.75	50	84.4	2.6	13.0	−10.4	0.18	264	950	1.6
0.8	50	88.9	1.4	9.7	−8.3	0.17	275	950	1.5
0.75	150	84.0	8.0	8.0	0.0	0.16	525	1350	1.8
				SH					
0.7	50	68.9	6.6	24.6	−18.0	0.19	327	900	1.2
0.75	50	62.8	7.0	30.2	−23.2	0.18	289	900	0.9
0.8	50	57.6	6.1	36.4	−30.3	0.18	325	850	0.7
0.75	150	44.5	11.1	44.4	−33.3	0.15	319	900	0.9

[a]In all cases $f_{nz} = 0.2$. The time step Δt is given in years. Percentage of time with semi-stationary events is denoted by 'St', percentage of time with eastward/westward drifts are denoted by 'Ea'/'We' respectively. The net drift is defined by Ne = Ea-We. The threshold distinguishing semi-stationary events from drifts is $\omega^e/2$. The RMS values of the absolute drift rates (denoted by 'Rate') are given in °/year. The average and longest lifetimes of patches τ_a and τ_m are given in years, and the average number of patches per snapshot is N_p. The analysis is given for each hemisphere, with northern/southern hemispheres denoted by NH/SH respectively.

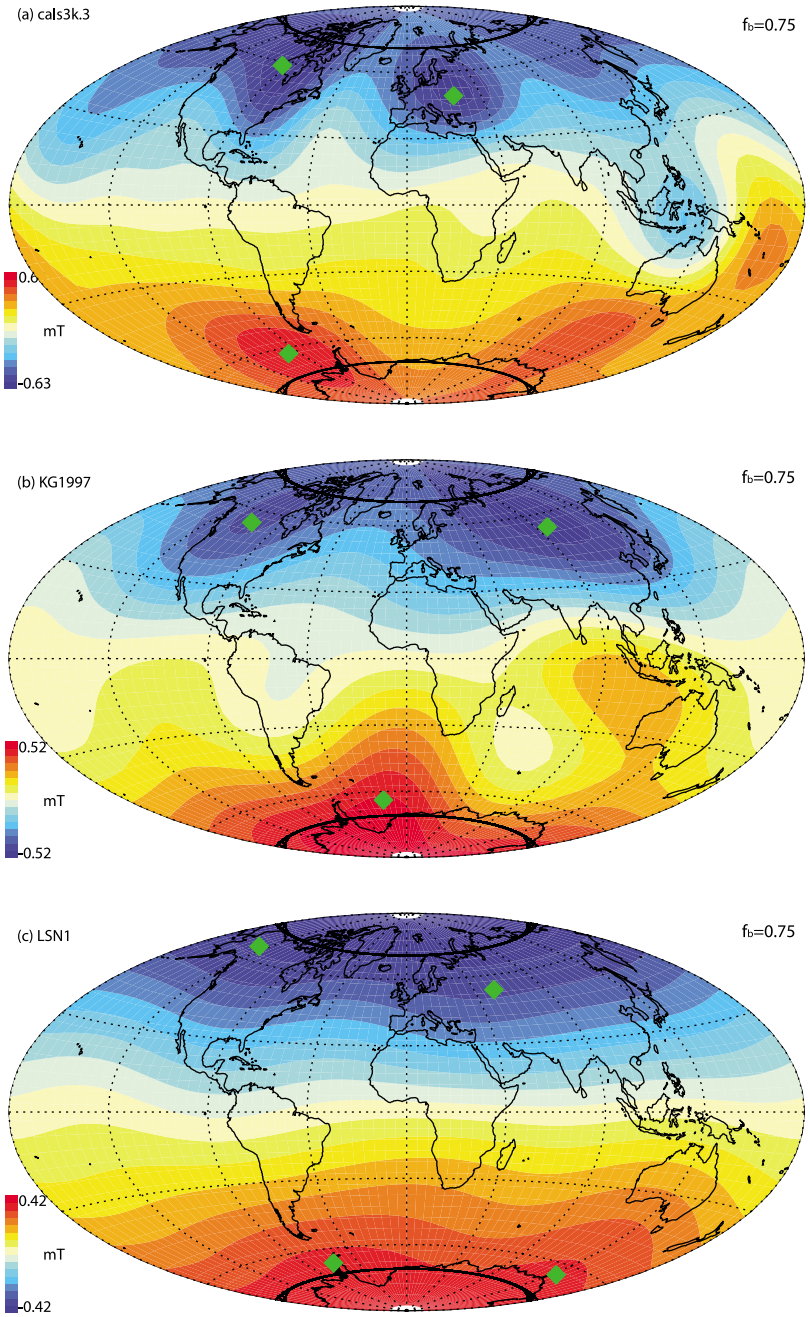

Figure 2. Time-average radial magnetic field on the CMB and the identified patches. (a) The archeomagnetic model *CALS3k.3* of *Korte et al.* [2009] for the past three millennia; (b) the paleomagnetic model of *Kelly and Gubbins* [1997] for the past five million years; (c) the paleomagnetic model *LSN1* of *Johnson and Constable* [1995] for the past five million years. In all cases we set $f_b = 0.75$ and $f_{nz} = 0.2$. Centers of identified patches are denoted by diamonds. Solid black lines mark the latitudes where the tangent cylinder intersects the CMB.

field between −1000 to 1850. For comparison, Figures 2b and 2c show the time-average paleomagnetic field models of *Kelly and Gubbins* [1997] and *Johnson and Constable* [1995] respectively. The identification method using the non-zonal criterion proves useful especially for the latter which has a very dominant axial dipole component. In this model indeed, if we only relied on criterion (1), patches would be falsely identified very close to the geographical poles. Instead, the non-zonal criterion enables identifying ridges that correspond to non-zonal deviations.

[14] Despite the very large time disparity, the locations of the patches in the time-average archeomagnetic and paleomagnetic field models display some similarity, although they also display some significant differences. The time-average archeomagnetic field shows two intense patches in the northern hemisphere and one in the southern hemisphere, all

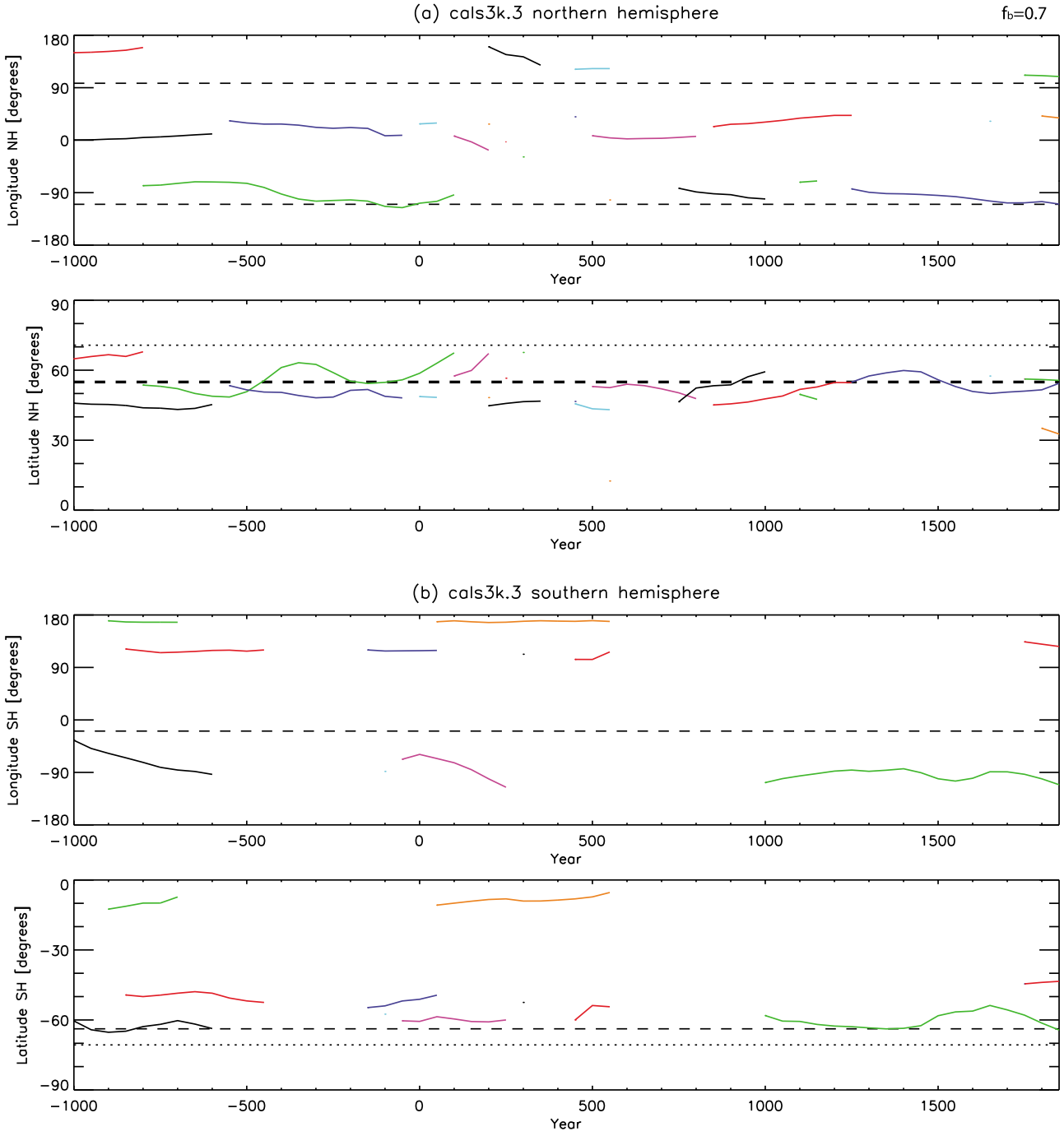

Figure 3. Time series of the longitude and latitude of the centers of mass of the intense patches (distinguished by different colors) in model *CALS3k.3* with $f_b = 0.7$ and $f_{nz} = 0.2$ in the (a) northern and (b) southern hemispheres. Coordinates units are in degrees. Dashed horizontal lines denote the coordinates of the patches identified in the time-average field of *Kelly and Gubbins* [1997] in each hemisphere (see Figure 2b). Dotted horizontal lines in the latitude (lower) subplots denote the tangent cylinder. As time progresses, each new color represents a new patch. For a given color, positive/negative trends correspond to eastward/westward patch drift in the longitude curves, or northward/southward in the latitude curves.

at high-latitudes near the edge of the tangent cylinder (Figure 2a). The paleomagnetic field model of *Kelly and Gubbins* [1997] also exhibits two patches in somewhat similar locations in the northern hemisphere and only one patch in the southern hemisphere (Figure 2b). In contrast, the paleomagnetic field model of *Johnson and Constable* [1995] has two patches in each hemisphere.

[15] The sensitivity of the results to the choice of the critical intensity threshold is examined by considering time series and synthetic analysis with $f_b = 0.7$ and $f_b = 0.8$. Comparison of Figures 3 and 4 and their corresponding values in Table 1

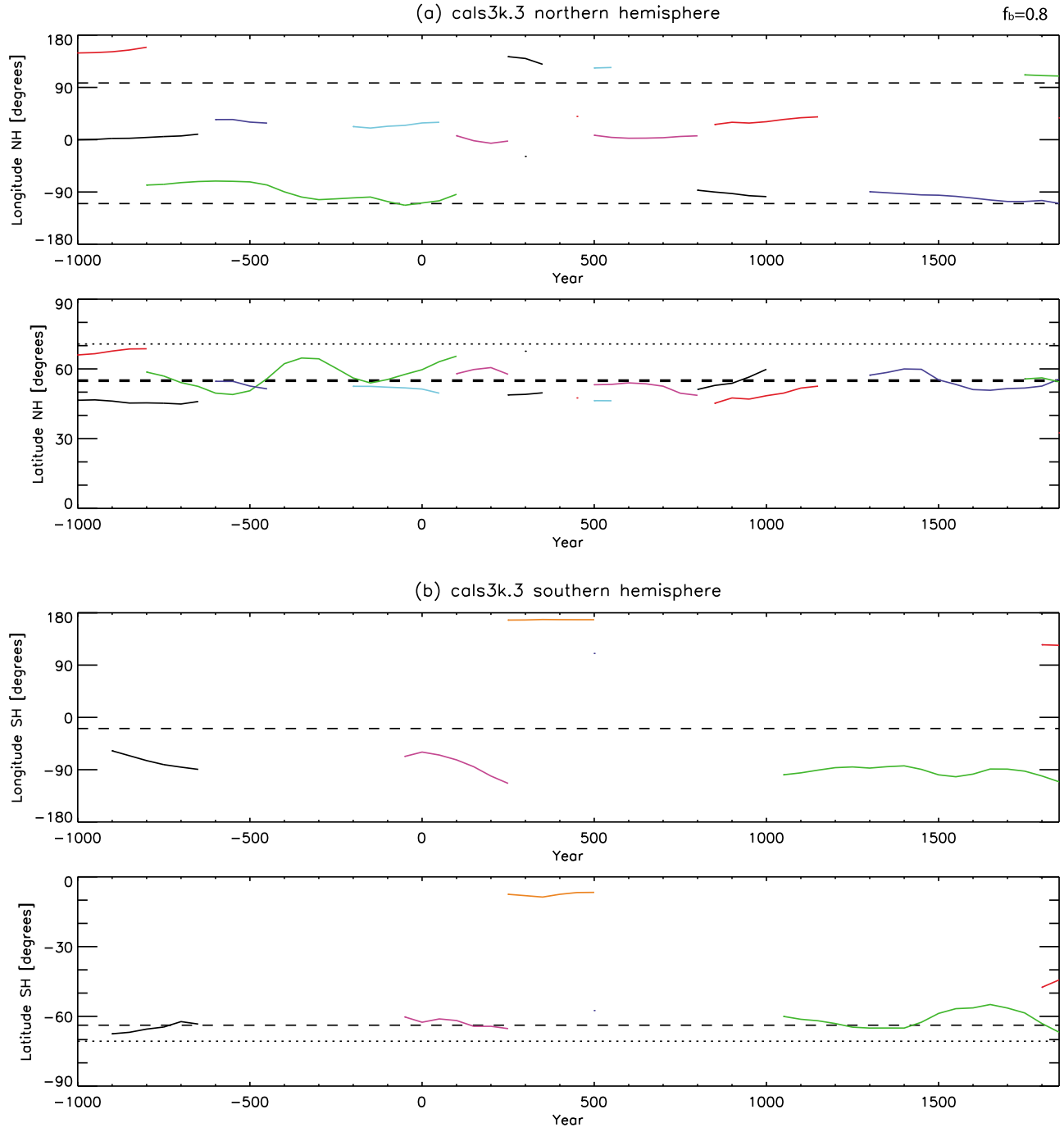

Figure 4. Sensitivity test: As in Figure 3 for $f_b = 0.8$.

shows that for larger f_b fewer patches are identified. However, the main trends and statistics are overall weakly dependent on the choice of f_b.

[16] A movie of the identified intense flux patches spanning the period −1000 to 1850 with f_b = 0.75 is given in Animation S1 of the auxiliary material (diamonds mark instantaneous patches, asterisks denote the time-average locations of the patches in the paleomagnetic field model of *Kelly and Gubbins* [1997]).[1] Figure 5 shows the corresponding time series of the patch coordinates in each hemisphere. We also visualize in Figure 6 the corresponding polar views of the patch trajectories in each hemisphere (each patch is denoted by the same color in Figures 5 and 6). Figures 5 and 6 clearly highlight the lower data sampling of the archeomagnetic field model in the southern hemisphere.

[17] To compare these results with those previously obtained by AAH10 with numerical dynamo models, we repeat our analysis by using a larger time step of Δt = 150 yrs (Table 1) to match the temporal data density of the dynamo models. Figure 7 compares the time series of the northern hemisphere longitude of the archeomagnetic field with

[1]Auxiliary materials are available in the HTML. doi:10.1029/2011JB008538.

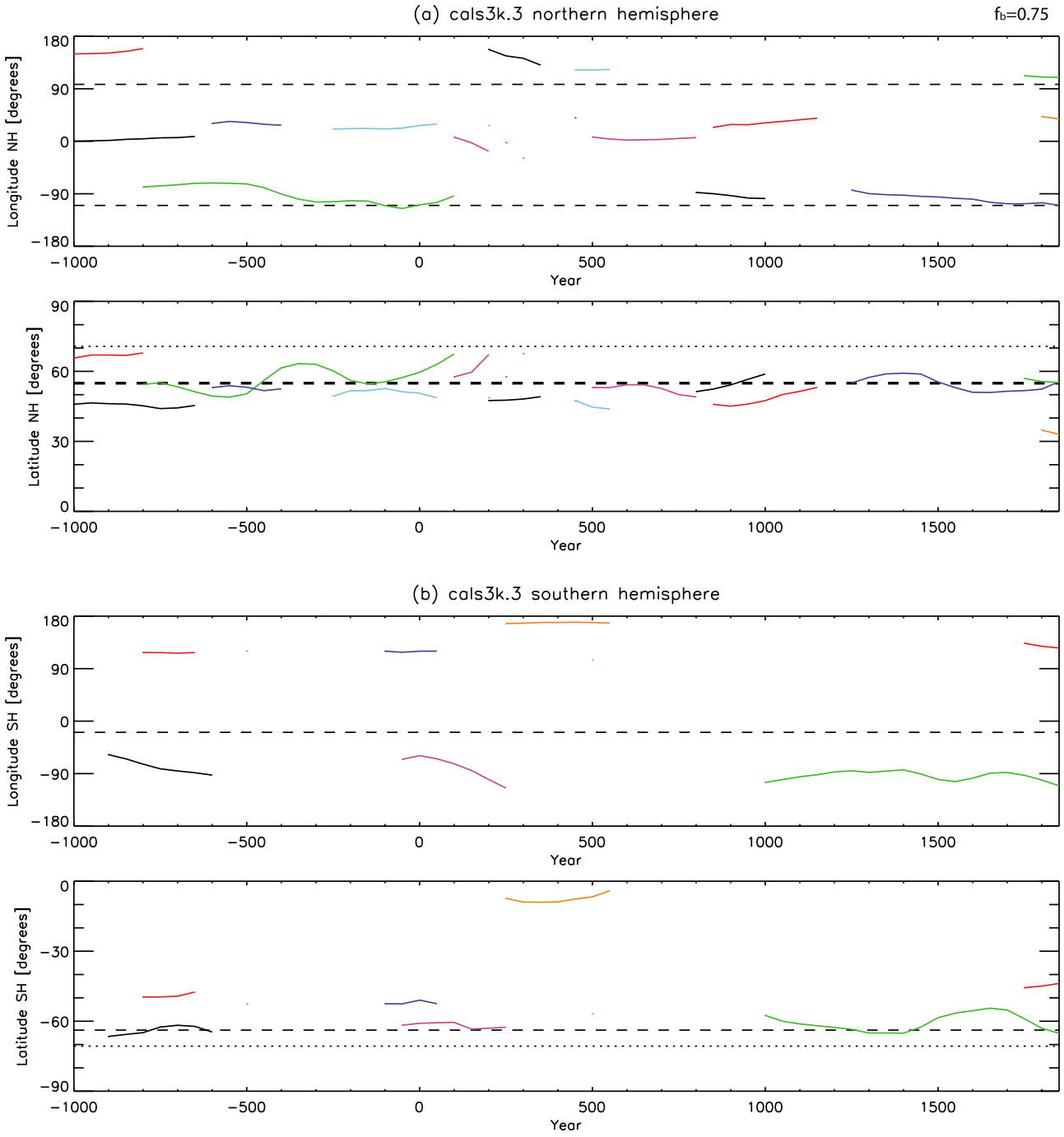

Figure 5. As in Figure 3 for $f_b = 0.75$.

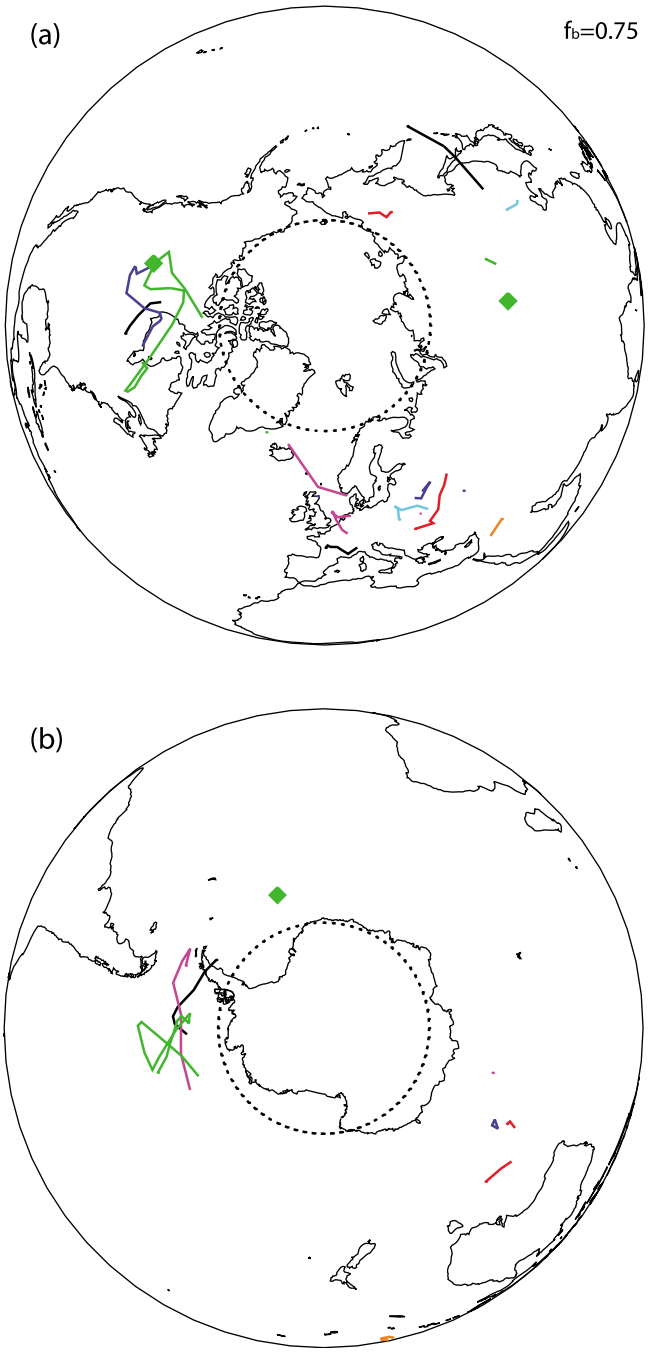

Figure 6. Polar views of patches trajectories corresponding to Figure 5. Dotted horizontal lines denote the tangent cylinder. Each patch has the same color as in Figure 5. The locations of the time-average paleomagnetic patches of *Kelly and Gubbins* [1997] are denoted by green diamonds.

corresponding time series of 3000 years intervals from case *Tolr* of AAH10 (which most resembles the statistics of the archeomagnetic field model, see Table 2). Note that time in the numerical dynamo models has been re-scaled compared to the original scaling used in AAH10. This is justified in section 4 where the comparison between the behavior of patches in the archeomagnetic field and numerical dynamos is discussed.

[18] We end the analysis of the archeomagnetic field model at 1850 and complete the temporal coverage with the higher resolution historical geomagnetic field model *gufm1* derived from direct measurements (including intensity) for the period 1840–1990. Animation S2 of the auxiliary material and Figure 8 demonstrate that the method performs adequately for the historical model as well. Note that the patches identified in the beginning of the historical period below North America, central Asia and southeast Pacific (Figure 9) also appear at the end of the archeomagnetic period (Figure 5), so the two geomagnetic field models exhibit continuity in the behavior of the patches. The 150-years period is very short for tracking significant time variability (Figure 9). Between 1840–1915 two high-latitude patches in the northern hemisphere and one in the southern hemisphere are present. In 1920 another high-latitude southern hemisphere patch is detected. In 1935 a low-latitude patch below Africa emerges. These five patches remain until 1985. In 1990 one high-latitude southern hemisphere structure weakens and loses its status as a patch.

4. Discussion

[19] We begin by comparing our results with previous studies that used different approaches to analyze the archeomagnetic field. *Dumberry and Finlay* [2007] found coherent azimuthal motions in the northern hemisphere, but practically none in the southern hemisphere, arguing that the low resolution of the archeomagnetic field model there prevents detecting non-zonal features. We also identify many fewer patches in the southern hemisphere, although some southern hemisphere patches are nevertheless detected. It is important to recall that the *CALS3k.3* archeomagnetic field model used here contains more data and spatial structure, especially in the southern hemisphere, than the model *CALS3k.2* used by *Dumberry and Finlay* [2007]. The direction of drift in our analysis alternates between eastward and westward, in agreement with *Dumberry and Finlay* [2007] and with *Wardinski and Korte* [2008]. The magnitude of ~0.2°/yr drift rates in our results is again in agreement with the rates reported by *Dumberry and Finlay* [2007].

[20] Interestingly, based on longitudinal cross-correlation, *Wardinski and Korte* [2008] found in some periods opposing trends in the northern/southern hemispheres. *Dumberry and Bloxham* [2006] also argued that the equatorial symmetry is broken on millennial timescales. This is in contradiction to equatorially symmetric columnar flow that is thought to prevail in Earth's core on shorter timescales due to the expected dominance of rotational effects [*Busse*, 1975; *Olson et al.*, 1999; *Jault*, 2008; *Pais and Jault*, 2008]. A pair of prominent intense flux patches in both hemispheres near 90°*W* (Figure 5) is possibly the surface expression of columnar flow. To test this hypothesis, we focus on periods in which both patches are simultaneously present in Figure 5. Between −800 to −600 and between −50 to 100 the northern patch moves eastward, whereas the southern generally moves westward. Between 1250 to 1850 the northern patch drifts westward, whereas the southern alternates between eastward and westward motions. Overall, these results do not support equatorial symmetry in the kinematics of intense flux patches. It is worth stressing, however, that the kinematics of the high-latitude intense flux patches does not necessarily reflect core flow, but could alternatively result from wave

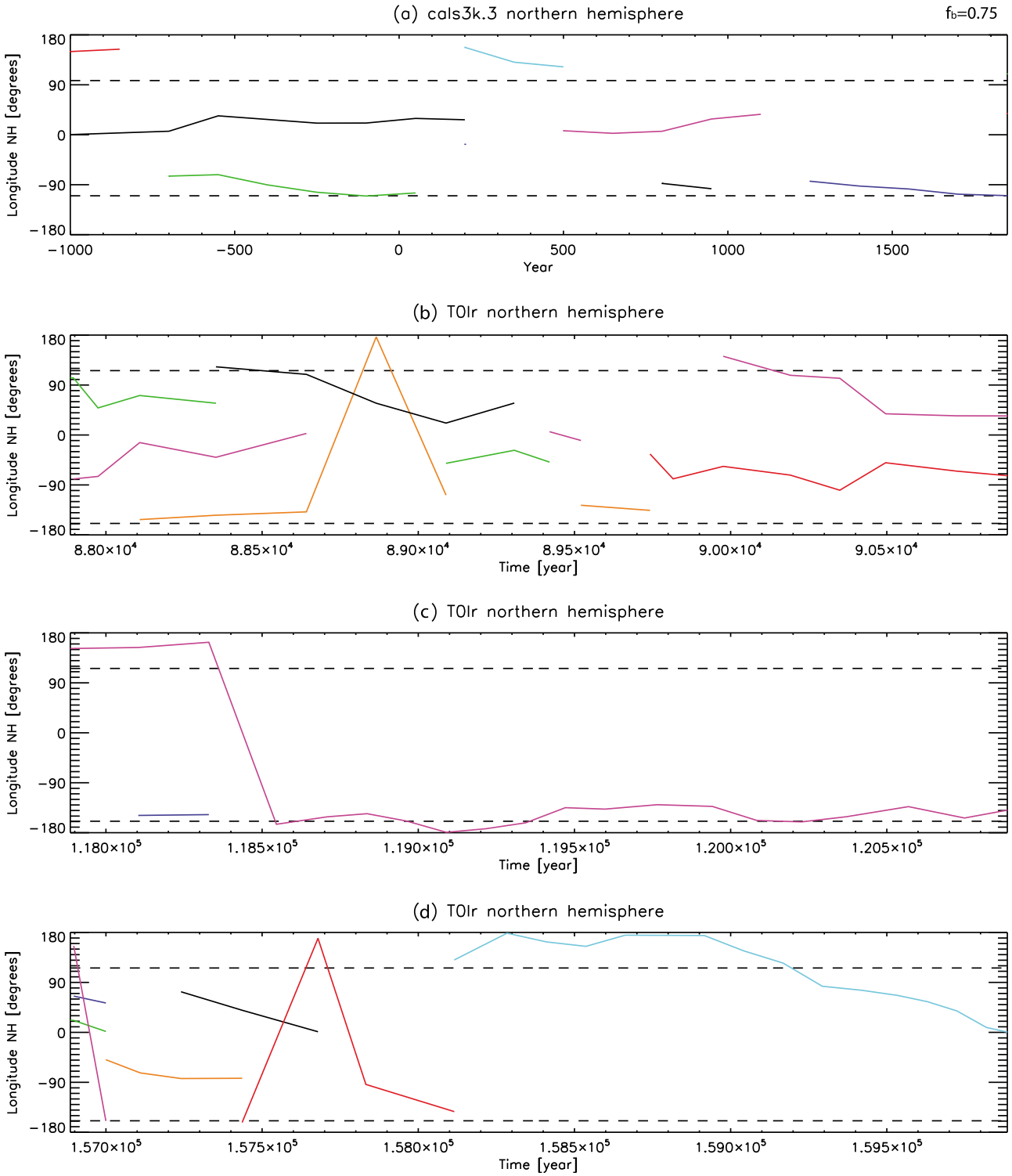

Figure 7. Comparison between (a) *CALS3k.3* and (b–d) the dynamo model *T0lr* of AAH10. In Figure 7a the model was down-sampled to $\Delta t = 150$ for compatibility with the sampling density in Figures 7b–7d. In Figures 7b–7d time was re-scaled by Rm/Rm^e compared to the original scaling used in AAH10 (see discussion for details). Only the time series of the northern hemisphere longitudes are shown. The dashed lines in Figure 7a represent the coordinates of intense flux patches in the time-average paleomagnetic field model of *Kelly and Gubbins* [1997], while in Figure 7b the dashed lines are the time-average coordinates in the numerical dynamo model.

Table 2. Synthetic Analysis of the Numerical Dynamos Time Series from AAH10[a]

Case	St	Ea	We	Ne	Rate	τ_a	τ_m
			NH				
T0lr	43.3	23.3	32.8	−9.5	0.20	298	6099
T0	52.5	28.1	19.4	8.7	0.15	653	3947
T0hr	52.9	22.1	25.0	−2.9	0.21	654	6020
T0hq	53.2	22.4	24.4	−2.0	0.15	819	7892
			SH				
T0lr	36.2	23.0	40.8	−17.8	0.21	251	2866
T0	49.7	19.9	30.4	−10.5	0.15	405	6135
T0hr	48.8	22.9	28.3	−5.4	0.21	590	4545
T0hq	40.0	19.2	40.8	−21.6	0.16	383	2885

[a]Time is however re-scaled by Rm/Rm^e with $Rm^e = 760$ compared to the original results of AAH10 (their Table 3). All quantities are defined as in Table 1, the threshold distinguishing semi-stationary events from drifts being also $\omega^e/2$.

propagation [*Braginsky*, 1972, 1974; *Braginsky and Burlatskaya*, 1979; *Finlay and Jackson*, 2003] or a combined effect of magnetic field advection and diffusion [*Bloxham*, 1986; *Bloxham and Gubbins*, 1986; *Amit and Christensen*, 2008; *Chulliat and Olsen*, 2010]. AAH10 argued that the drift of the patches in their dynamo models corresponds to azimuthal propagation of fluid downwelling structures that concentrate the magnetic field on the CMB. Therefore caution should be taken in interpreting lack of equatorial symmetry in patches temporal behavior as lack of equatorial symmetry in core flow.

[21] The oscillatory motion of patches around a preferred location (Figures 5 and 6) may be related to the phenomenon of archeomagnetic jerks, which are defined as sharp regional directional variations and intensity maxima in the archeomagnetic field [*Gallet et al.*, 2003]. *Dumberry and Finlay* [2007] speculated that archeomagnetic jerks occur when intense patches change the direction of their azimuthal oscillation. The occurrence times of archeomagnetic jerks determined from French archeomagnetic data have been summarized by *Gallet et al.* [2003] as approximately −800, 200, 800, 1400 and perhaps 500 and 1600. Comparison of these times with the movement of northern hemisphere flux lobes from our analysis (Figure 5) does not show a systematic relation between archeomagnetic jerks and flux patches directional change of motion. The proposed times of archeomagnetic jerks seem to coincide with times of significant intensification or weakening of regional magnetic flux, when our detection method respectively begins or ends classifying the features as intense flux patches. The emergence or disappearance of a patch could thus be related to archeomagnetic jerks, possibly by contributing to build the hemispherical asymmetry of the field [*Gallet et al.*, 2008].

[22] We now turn to compare the behavior of the patches in the archeomagnetic field and in the numerical dynamos investigated by AAH10 (Figure 7). As already noted, this comparison requires appropriate re-scaling of the time in the simulations of AAH10. Re-dimensionalization of time in numerical dynamos is indeed non-unique [*Christensen and Wicht*, 2007]. AAH10 used the magnetic diffusion time to re-scale time in their dynamo models. However, as recently emphasized by *Lhuillier et al.* [2011], re-scaling dynamo model time by using secular variation timescales [*Hulot and LeMouël*, 1994] may be much more appropriate for comparisons with geomagnetic observations. Such re-scaling amounts to introducing a factor of Rm/Rm^e to the time used by AAH10 [*Christensen and Tilgner*, 2004]. Using $Rm^e = 760$ for Earth's core (taking into account the definition of Rm used by AAH10 [*Christensen and Tilgner*, 2004]) we obtain in Table 2 the same order of magnitude of drift rates and approach similar average lifetimes in the archeomagnetic field studied here and in the numerical dynamo models of AAH10. Case *Tolr* of AAH10 is closest in its τ_a value to the archeomagnetic field, so we compare intervals of 3000 (re-scaled) years from this model with the analysis of the archeomagnetic field (see Figure 7).

[23] Our analysis shows that the archeomagnetic field shares some common features with the field produced by the tomographic numerical dynamos of AAH10. The patches in the archeomagnetic field model appear near the edge of the tangent cylinder. One exception is a patch below equatorial western Pacific between 350 to 500 (orange line in Figure 5b). This patch could be related to the intense low-latitude flux patches observed in the historical field [*Jackson*, 2003], one of which below Africa is classified as intense by our algorithm (Figures 8 and 9). Even though our analysis reveals

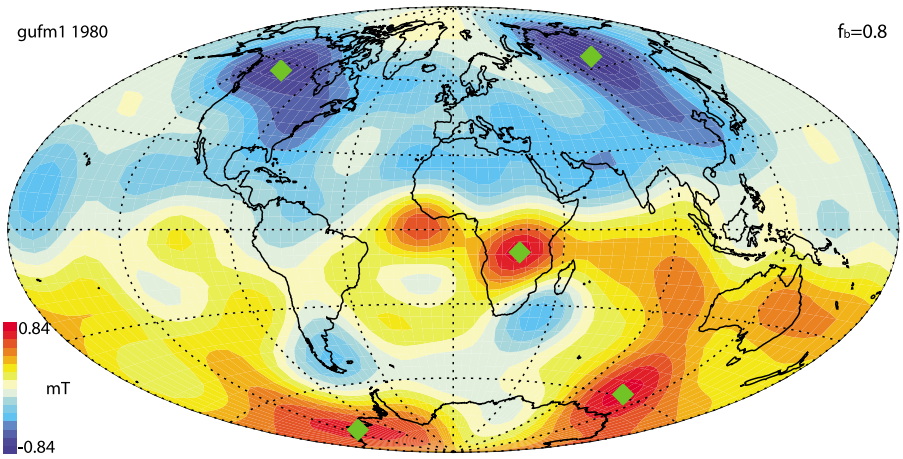

Figure 8. Patches identification in the radial geomagnetic field of 1980 from *gufm1* [*Jackson et al.*, 2000] with $f_b = 0.8$ and $f_{nz} = 0.2$.

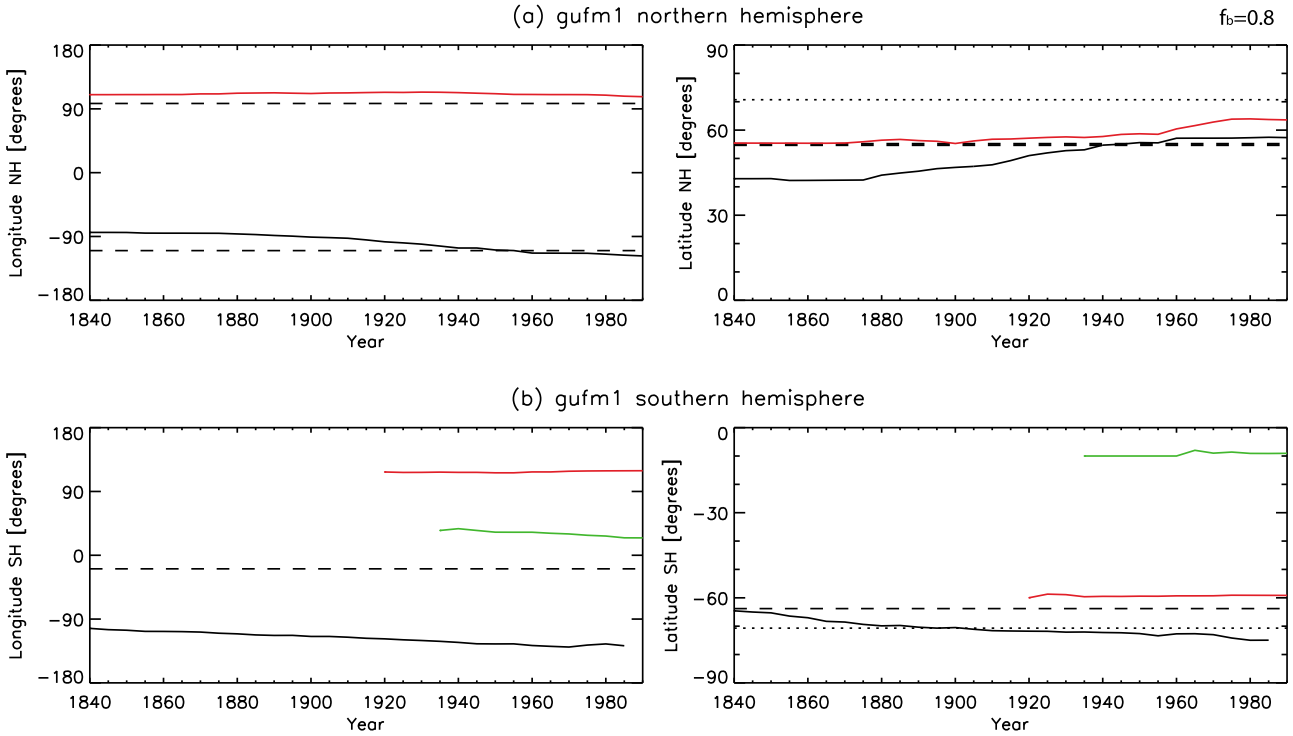

Figure 9. Time series of the longitude and latitude of the centers of mass of intense patches (distinguished by different colors) in model *gufm1* with $f_b = 0.8$ and $f_{nz} = 0.2$ in the (a) northern and (b) southern hemispheres. Coordinates units are in degrees. Dashed horizontal lines denote the coordinates of the patches identified in the time-average field of *Kelly and Gubbins* [1997] in each hemisphere (see Figure 2b). Dotted horizontal lines in the latitude plots denote the tangent cylinder. As time progresses, each new color represents a new patch. For a given color, positive/negative trends correspond to eastward/westward patch drift in the longitude curves, or northward/southward in the latitude curves.

somewhat less mobility in the archeomagnetic field models than in the numerical dynamos (see larger St values in Table 1 than in Table 2), Figure 7 shows that the dynamo models can exhibit some periods with similar behavior characterized by intense patches also residing away from their long term time-average coordinates. Several archeomagnetic patches in Figure 7a oscillate about the time-average paleomagnetic flux patch below north America (Figure 2b), whereas the other patches are relatively distant from the Asian paleomagnetic patch. A similar behavior is seen in case *T0lr* of AAH10 during the zoom-in of Figure 7b, where intense patches are often found in between the preferred long term time-average locations. At other times (e.g., in Figure 7c) these patches appear to be near their time-average locations, just like over the past centuries the geomagnetic field patches locations appear near the time-average paleomagnetic flux patches seen in the northern hemisphere (Figure 9). These observations support a statistical behavior proposed by AAH10 in which locations of high-latitude patches roughly coincide with that of the time-average paleomagnetic field while the latter appears to be much weaker.

[24] Finally, it is worth pointing out that in the archeomagnetic field westward drift occurs more often than eastward. Moreover, the net drift is much more negative (i.e. more westward) in the southern hemisphere than in the northern. Although the southern hemisphere contains fewer identified patches (probably due to lower data sampling and resolution there), the few drift events are often westward (see black curve between −900 to −600 and purple curve between 0 to 250 in Figure 5b), whereas the northern hemisphere is more balanced (Figure 5a). The hemispheric dichotomy in the net drift is in agreement with time-average core flow models inferred from inversions of geomagnetic SV data [*Pais and Hulot*, 2000; *Amit and Olson*, 2006] and supports the speculation of AAH10 that mantle-driven thermal wind may cause stronger time-dependence of patches and weaker paleomagnetic patches in the southern hemisphere.

[25] In contrast to the results of AAH10, no patch is observed completing a full drift from one preferred location to another. Zoom-ins of the dynamo models also rarely show a full drift from one preferred location to another within a period of 3000 years, but a tendency for such a mobility can sometimes be identified (see e.g. Figure 7d). In addition, the average lifetime of a patch τ_a is longer in the southern hemisphere than in the northern, again in contrast with the findings of AAH10. The latter discrepancy could be due to low archeomagnetic data resolution in the southern hemisphere.

[26] It is worth-while comparing the average lifetime $\tau_a \sim$ 300 years with other analyses of archeomagnetic field models and with some theoretical expected values. *Dumberry and Finlay* [2007] found that a period of about 100 years is required to change the azimuthal drift direction, while the duration of a drift event is about a few hundred years. *Wardinski and Korte* [2008] found an average dominant period of 800 years in their inverted core flows. The study of *Dumberry and Bloxham* [2006], which tried to relate

zonal flows reconstructed from archeomagnetic field models with length of day variations, also provide a timescale of approximately 800 years for drift events. AAH10 argued that the time-dependence of intense magnetic flux patches is related to the motion of fluid downwelling structures that concentrate magnetic flux. Vortices may either split when entering a shear zone, or merge when approaching other vortices. The magnetic field passively responds by splitting and merging with the vortex evolution. If that is the case, the average lifetime of $\tau_a \sim 300$ years may be related to vortex lifetime in the outer core.

5. Summary

[27] Identifying and tracking intense archeomagnetic field structures provides insight into the working of the geodynamo over millennial timescales. Here we applied the method of AAH10 on the recent field model *CALS3k.3*. As in the historical (e.g. *gufm1*) and some paleomagnetic [e.g., *Kelly and Gubbins*, 1997] field models, we also find that intense flux patches reside at high-latitudes close to the tangent cylinder. The patches usually oscillate about some longitudes rather than exhibit strictly monotonous drifts. The direction of the motions alternate between eastward and westward, but more westward drift is observed, especially in the southern hemisphere. The latter result is in agreement with some core flow inversions from the historical geomagnetic SV [*Pais and Hulot*, 2000; *Amit and Olson*, 2006] and numerical dynamos with tomographic boundary conditions (AAH10), indicating that the pattern of the zonal core flow is possibly influenced by lower mantle heterogeneity.

[28] In this study we argue that the nature of time-dependence of high-latitude intense geomagnetic flux patches inferred from archeomagnetic field models is in agreement with the same scenario proposed before by AAH10 based on numerical dynamo models. The temporal variability of these patches is comprised of statistically longer periods near preferred locations represented by the long term time-average paleomagnetic field, providing some likelihood for the present geomagnetic flux patches to correlate with the paleomagnetic patches. However, the patches are mobile enough and can be found at times far from these preferred locations, hence resulting in the weaker non-dipole signature in the paleomagnetic field with respect to the present geomagnetic field.

[29] As in previous studies of archeomagnetic field models [e.g., *Dumberry and Finlay*, 2007; *Wardinski and Korte*, 2008], our analysis clearly suffers from low statistical sampling, both in space and in time. It is therefore possible, for example, that in some cases appearances and disappearances of patches might be caused by incomplete data distribution, although such biases seem unlikely because several sediment records span the whole time interval. To confirm the robustness of our findings, higher resolution archeomagnetic field models are required. Especially in the southern hemisphere, more records are needed to resolve more detailed structure. Improving archeomagnetic field models clearly poses a high-priority challenge for better probing the behavior of the geodynamo.

[30] **Acknowledgments.** C.C. acknowledges support from NSF grant EAR 0809709. We thank Mathieu Dumberry and an anonymous reviewer for their constructive comments that improved this manuscript. This study was partly supported by CNES. This is IPGP contribution 3243.

References

Amit, H., and U. Christensen (2008), Accounting for magnetic diffusion in core flow inversions from geomagnetic secular variation, *Geophys. J. Int.*, *175*, 913–924.

Amit, H., and P. Olson (2006), Time-average and time-dependent parts of core flow, *Phys. Earth Planet. Inter.*, *155*, 120–139.

Amit, H., J. Aubert, and G. Hulot (2010), Stationary, oscillating or drifting mantle-driven geomagnetic flux patches?, *J. Geophys. Res.*, *115*, B07108, doi:10.1029/2009JB006542.

Aubert, J., H. Amit, G. Hulot, and P. Olson (2008), Thermo-chemical flows couple the Earth's inner core growth to mantle heterogeneity, *Nature*, *454*, 758–761.

Bloxham, J. (1986), The expulsion of magnetic flux from the Earth's core, *Geophys. J. R. Astron. Soc.*, *87*, 669–678.

Bloxham, J. (2002), Time-independent and time-dependent behaviour of high-latitude flux bundles at the core-mantle boundary, *Geophys. Res. Lett.*, *29*(18), 1854, doi:10.1029/2001GL014543.

Bloxham, J., and D. Gubbins (1986), Geomagnetic field analysis - IV. Testing the frozen-flux hypothesis, *Geophys. J. R. Astron. Soc.*, *84*, 139–152.

Bloxham, J., and A. Jackson (1991), Fluid flow near the surface of the Earth's outer core, *Rev. Geophys.*, *29*, 97–120.

Braginsky, S. (1972), Analytical description of geomagnetic field of the past and spectral analysis of magnetic waves in the Earth's core, *Geomagn. Aeron.*, *12*, 1092–1105.

Braginsky, S. (1974), Analytical description of geomagnetic field of the past and spectral analysis of magnetic waves in the Earth's core II, *Geomagn. Aeron.*, *14*, 522–529.

Braginsky, S., and S. Burlatskaya (1979), Spherical analysis of the geomagnetic field based on archeomagnetic data, *Izv. Akad. Nauk. SSSR, Ser. Fiz.*, *15*, 891–895.

Busse, F. (1975), A model of the geodynamo, *Geophys. J. R. Astron. Soc.*, *42*, 437–459.

Christensen, U., and A. Tilgner (2004), Power requirement of the geodynamo from ohmic losses in numerical and laboratory dynamos, *Nature*, *439*, 169–171.

Christensen, U., and J. Wicht (2007), Numerical dynamo simulations, in *Treatise on Geophysics*, vol. 8, edited by P. Olson, pp. 245–282, Elsevier Sci., New York.

Christensen, U., P. Olson, and G. Glatzmaier (1998), A dynamo model interpretation of geomagnetic field structures, *Geophys. Res. Lett.*, *25*, 1565–1568.

Christensen, U., J. Aubert, and G. Hulot (2010), Conditions for Earth-like geodynamo models, *Earth Planet. Sci. Lett.*, *296*, 487–496.

Chulliat, A., and N. Olsen (2010), Observation of magnetic diffusion in the Earth's outer core from Magsat, Orsted and CHAMP data, *J. Geophys. Res.*, *115*, B05105, doi:10.1029/2009JB006994.

Constable, C., C. Johnson, and S. Lund (2000), Global geomagnetic field models for the past 3000 years: Transient or permanent flux lobes?, *Philos. Trans. R. Soc. A*, *358*, 991–1008.

Dumberry, M., and J. Bloxham (2006), Azimuthal flows in the Earth's core and changes in the length of day at millennial timescales, *Geophys. J. Int.*, *165*, 32–46.

Dumberry, M., and C. Finlay (2007), Eastward and westward drift of the Earth's magnetic field for the last three millennia, *Earth Planet. Sci. Lett.*, *254*, 146–157.

Finlay, C., and A. Jackson (2003), Equatorially dominated magnetic field change at the surface of Earth's core, *Science*, *300*, 2084–2086.

Gallet, Y., A. Genevey, and V. Courtillot (2003), On the possible occurrence of archeomagnetic jerks in the geomagnetic field over the past three millennia, *Earth Planet. Sci. Lett.*, *214*, 237–242.

Gallet, Y., G. Hulot, A. Chulliat, and A. Genevey (2008), Geomagnetic field hemispheric asymmetry and archeomagnetic jerks, *Earth Planet. Sci. Lett.*, *284*, 179–186.

Gubbins, D., P. Willis, and B. Sreenivasan (2007), Correlation of Earth's magnetic field with lower mantle thermal and seismic structure, *Phys. Earth Planet. Inter.*, *162*, 256–260.

Hulot, G., and J.-L. LeMouël (1994), A statistical approach to the Earth's main magnetic field, *Phys. Earth Planet. Inter.*, *82*, 167–183.

Jackson, A. (2003), Intense equatorial flux spots on the surface of the Earth's core, *Nature*, *424*, 760–763.

Jackson, A., A. Jonkers, and M. Walker (2000), Four centuries of geomagnetic secular variation from historical records, *Philos. Trans. R. Soc. A*, *358*, 957–990.

Jault, D. (2008), Axial invariance of rapidly varying diffusionless motions in the Earth's core interior, *Phys. Earth Planet. Inter.*, *166*, 67–76.

Johnson, C., and C. Constable (1995), The time averaged geomagnetic field as recorded by lava flows over the past 5 myr, *Geophys. J. Int.*, *122*, 489–519.

Kelly, P., and D. Gubbins (1997), The geomagnetic field over the past 5 million years, *Geophys. J. Int.*, *128*, 315–330.

Korte, M., and C. Constable (2003), Continuous global geomagnetic field models for the past 3000 years, *Phys. Earth Planet. Inter.*, *140*, 73–89.

Korte, M., and C. Constable (2005), Continuous geomagnetic models for the past 7 millennia: 2. Cals7k., *Geochem. Geophys. Geosyst.*, *6*, Q02H16, doi:10.1029/2004GC000801.

Korte, M., and R. Holme (2010), On the persistence of geomagnetic flux lobes in global field models, *Phys. Earth Planet. Inter.*, *182*, 179–186.

Korte, M., F. Donadini, and C. Constable (2009), The geomagnetic field for 0–3 ka: 2. A new series of time-varying global models, *Geochem. Geophys. Geosyst.*, *10*, Q06008, doi:10.1029/2008GC002297.

Labrosse, S. (2002), Hotspots, mantle plumes and core heat loss, *Earth Planet. Sci. Lett.*, *199*, 147–156.

Lhuillier, F., A. Fournier, G. Hulot, and J. Aubert (2011), The geomagnetic secular-variation timescale in observations and numerical dynamo models, *Geophys. Res. Lett.*, *38*, L09306, doi:10.1029/2011GL047356.

Masters, G., G. Laske, H. Bolton, and A. Dziewonski (2000), The relative behavior of shear velocity, bulk sound velocity, and compressional velocity in the mantle: Implications for chemical and thermal structure, in *Earths Deep Interior, Geophys. Monogr. Ser.*, vol. 117, edited by S. Karato et al., pp. 63–87, AGU, Washington D. C.

Olson, P., and U. Christensen (2002), The time averaged magnetic field in numerical dynamos with nonuniform boundary heat flow, *Geophys. J. Int.*, *151*, 809–823.

Olson, P., U. Christensen, and G. Glatzmaier (1999), Numerical modeling of the geodynamo: Mechanisms of field generation and equilibration, *J. Geophys. Res.*, *104*, 10,383–10,404.

Pais, A., and G. Hulot (2000), Length of day decade variations, torsional oscillations and inner core superrotation: Evidence from recovered core surface zonal flows, *Earth Planet. Sci. Lett.*, *118*, 291–316.

Pais, M. A., and D. Jault (2008), Quasi-geostrophic flows responsible for the secular variation of the Earth's magnetic field, *Geophys. J. Int.*, *173*, 421–443, doi:10.1111/j.1365–246X.2008.03741.x.

Wardinski, I., and M. Korte (2008), The evolution of the core-surface flow over the last seven thousands years, *J. Geophys. Res.*, *113*, B05101, doi:10.1029/2007JB005024.

Willis, P., B. Sreenivasan, and D. Gubbins (2007), Thermal core-mantle interaction: Exploring regimes for 'locked' dynamo action, *Phys. Earth Planet. Inter.*, *165*, 83–92.

H. Amit, Laboratoire de Planétologie et de Géodynamique, Université de Nantes, CNRS UMR 6112, 2 rue de la Houssinière, F-44000 Nantes, France. (Hagay.Amit@univ-nantes.fr)

J. Aubert, Equipe de Dynamique des Fluides Géologiques, Institut de Physique du Globe de Paris, Sorbonne Paris Cité, Université Paris Diderot, INSU, CNRS, UMR 7154, 1 rue Jussieu, F-75238 Paris, CEDEX 5, France.

C. Constable, Institute for Geophysics and Planetary Physics, Scripps Institution of Oceanography, University of California, 9500 Gilman Dr., San Diego, La Jolla, CA 92093-0225, USA.

G. Hulot, Equipe de Géomagnétisme, Institut de Physique du Globe de Paris, Sorbonne Paris Cité, Université Paris Diderot, INSU, CNRS, UMR 7154, 1 rue Jussieu, F-75238 Paris, CEDEX 5, France.

M. Korte, Helmholtz-Zentrum Potsdam, Deutsches GeoForschungsZentrum, Telegrafenberg, D-14473 Potsdam, Germany.